Supplemental Material

Tracking Thermal-Induced Amorphization of a Zeolitic Imidazolate Framework via Synchrotron In Situ Far-Infrared Spectroscopy

Matthew R. Ryder,[a,b] Thomas D. Bennett,[c] Chris S. Kelley,[b] Mark D. Frogley,[b] Gianfelice Cinque,[b] Jin-Chong Tan[a]

[a]*Department of Engineering Science, University of Oxford, Parks Road, Oxford OX1 3PJ, United Kingdom*

[b]*Diamond Light Source, Harwell Campus, Didcot, Oxford OX11 0DE, United Kingdom*

[c]*Department of Materials, University of Cambridge, Cambridge CB3 0FS, United Kingdom*

**Correspondence to*: jin-chong.tan@eng.ox.ac.uk

Table of Contents

1 Materials Synthesis and Characterization

The ZIF-4 sample was synthesized and evacuated according to the synthetic procedure in our previous work.[1, 2]

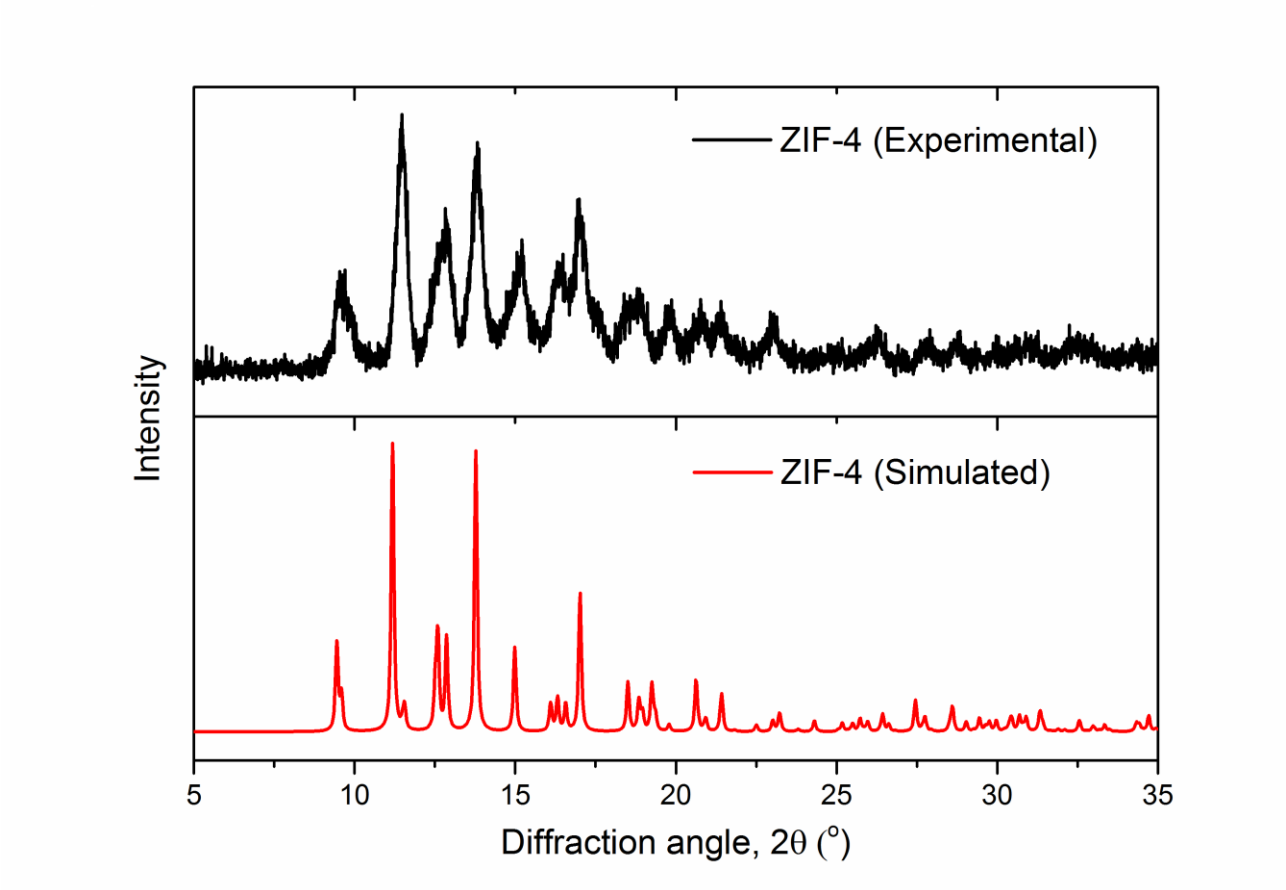

Fig. S1. Powder X-Ray Diffraction of ZIF-4 comparing the experimental spectrum for the sample used in the measurements and the simulated spectrum from the CIF file in the literature.[3]

The ZIF-8 sample was purchased from Sigma-Aldrich, Basolite® Z1200.

2 Synchrotron Radiation Far-Infrared (SR FIR) Absorption

The Far-infrared (FIR) absorption spectroscopy experiments were performed at the Multimode InfraRed Imaging and Microspectroscopy (MIRIAM) Beamline (B22) at the Diamond Light Source synchrotron facility.[4] One of the primary motivations to use synchrotron radiation (SR) was the increased brightness of the beam (photon flux density significantly higher than conventional sources). Therefore allowing for us to obtain high signal-to-noise data of the FIR spectral region.

The specific experimental setup was similar to that used by Greenaway *et al.* for the *in situ* mid-infrared microspectroscopy of CO_2 adsorption on single crystals of functionalized Sc-MOFs.[5] The work contained in this paper concentrated on the far-infrared spectral region via the utilization of a multilayer coated 6-micron mylar beamsplitter, and an IR Labs liquid helium cooled Si bolometer.

A small quantity of ZIF-4 powder was loaded on the heat stage of the Linkam cell, and the cell was sealed with an IR grade double polished Si window and mounted onto the microscope. There was a constant flow of nitrogen, and the sample was allowed to equilibrate for approximately 5 minutes at each temperature point. The following settings were used to obtain the spectral data:

Data Acquisition Parameters		
Optical Aperture		6 mm
Scanner Velocity		40 Hz
Spectral Resolution		2 cm^{-1}
Phase Resolution		16 Hz
Number of Scans*	ZIF-4	256
	ZIF-8	64

*The number of scans obtained for the ZIF-8 spectral measurements was less due to time constraints at the end of the beamtime.

3 *Ab Initio* Quantum Mechanical Calculations

All density functional theory (DFT) calculations were performed using the periodic *ab initio* code CRYSTAL14.[6] The vibrational frequencies and elastic constants of ZIF-zni were calculated using the exact methodology and computational parameters from our previous work of the THz vibrations of ZIFs[2] and the elasticity of unsubstituted imidazole containing ZIFs[7] respectively.

The theoretical IR spectra were calculated at the PBE level of theory[8] and corrected with an empirical Grimme dispersion term (PBE-D).[9] The mass-weighted Hessian matrix for the calculation of the vibrational frequencies was obtained by numerical differentiation of the analytical first derivatives, calculated at geometries obtained by displacing each of the 3N atomic coordinates of the equilibrium geometry. All electron TZVP basis sets were used for all atoms, the same as our previous work on the THz vibrations of ZIFs.[2]

The elastic constants were calculated at the B3LYP level of theory.[10] This allowed for the mechanical properties of ZIF-zni to be obtained via tensorial analysis as described in detail in our previous work on the mechanical properties of MOFs.[7, 11, 12]

4 ZIF-4 Peak Fitting and Spectral Curve Fitting

The peaks located in the 250-350 cm^{-1} spectral region were fitted using a Gaussian in the OriginPro 9.1 software. The result can be seen below for the room temperature spectrum. The error values were within a range comparable to the size of the symbols used in Figure 3 of the main text and hence error bars were unnecessary.

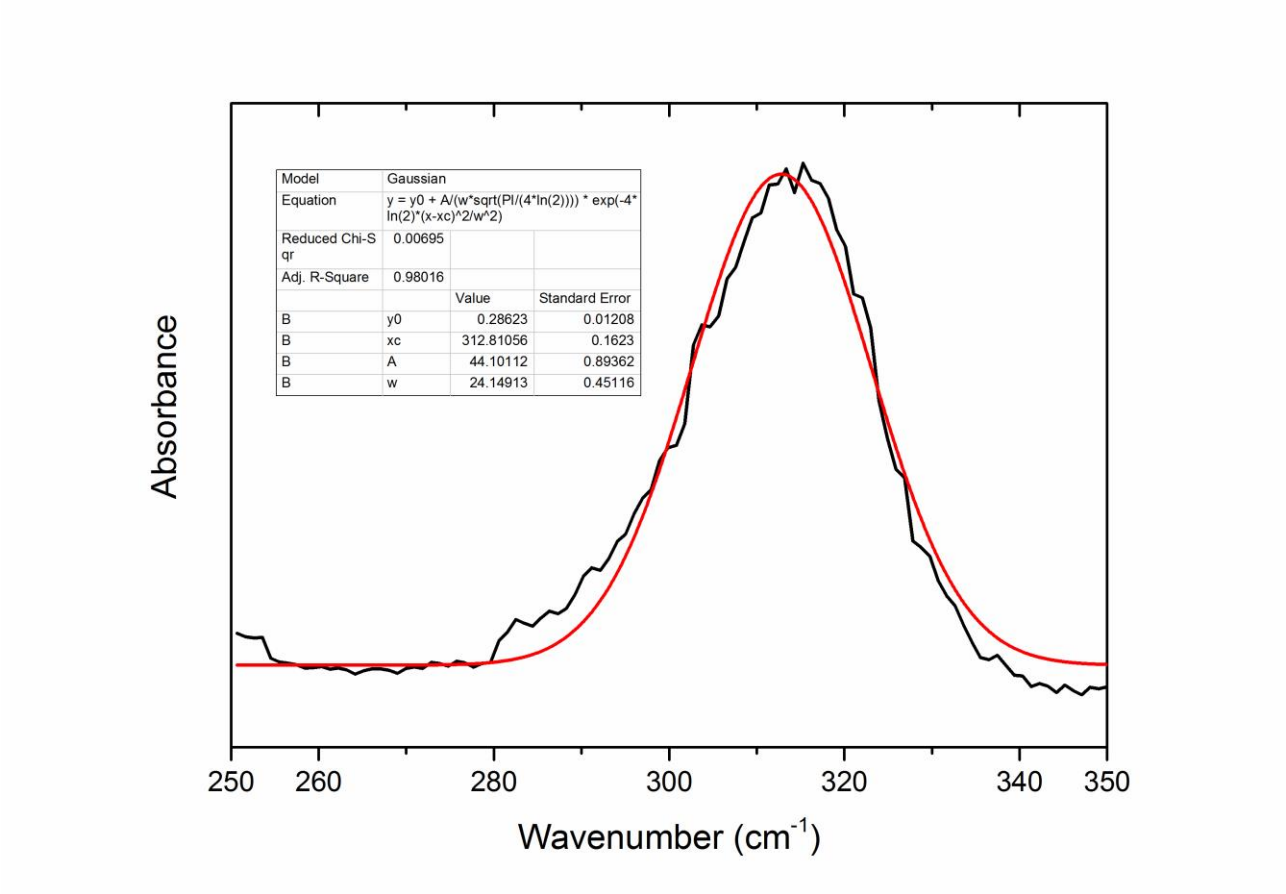

Fig. S2. Spectrum showing the fitting method for the 298 K peak of ZIF-4.

The curve fitting was also performed using the OriginPro 9.1 software from the equation stated in the main text:

$$\nu(T) = \nu_0 - \frac{X_R T_C}{e^{\frac{T_C}{T}} - 1}$$

$$T_C = \frac{h\nu_0}{k_B}$$

This yielded the X_R values that are stated in the text. The resultant values with associated errors for each tetrahedral environment are shown below.

Curve Fitting				
Tetrahedra	X_R	*Standard Error*	*Adj. R-Squared*	*Reduced Chi-Square*
$Zn(Im)_4$	0.04541	8.19764E-4	0.97001	1.19234
$Zn(mIm)_4$	0.03152	3.91277E-4	0.99515	0.13183

5 Young's Modulus 3-D Plot for ZIF-zni

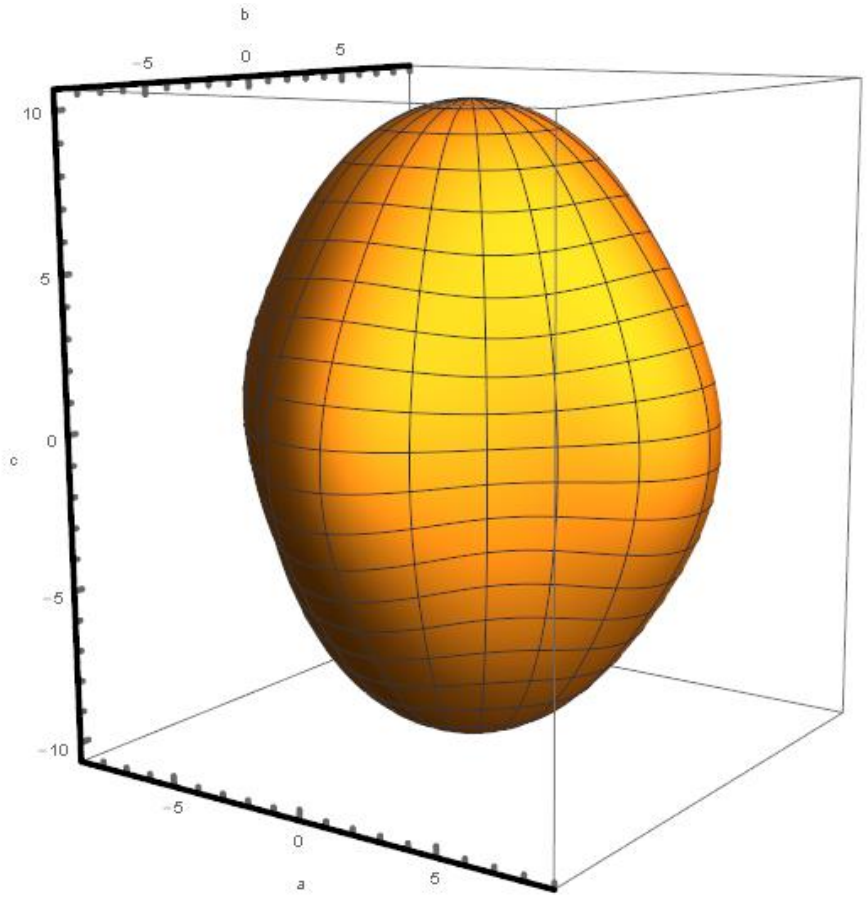

Figure. S3. 3-D Young's modulus representation surface $E(\theta, \varphi)$ of ZIF-zni in GPa.

6 Shear Modulus 3-D Plot for ZIF-zni

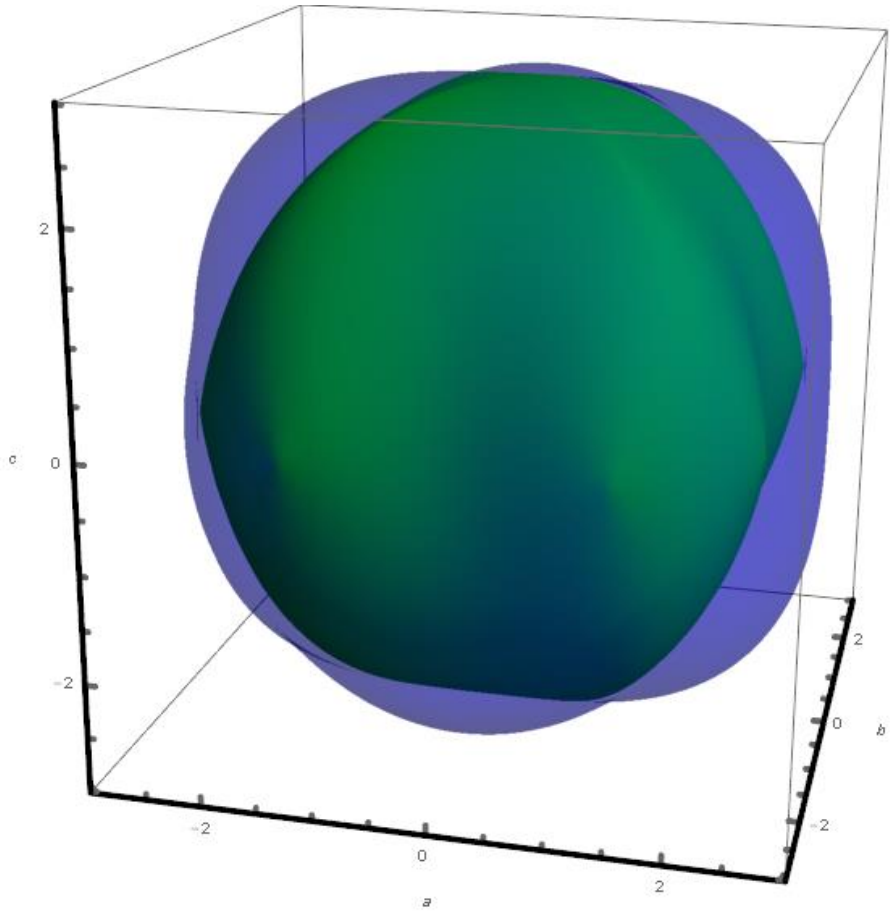

Figure. S4. 3-D shear modulus representation surface *G(θ, φ, χ)* of ZIF-zni. Colour coding used: blue and green represent the maximum and minimum moduli in GPa.

7 Linear Compressibility 3-D Plot for ZIF-zni

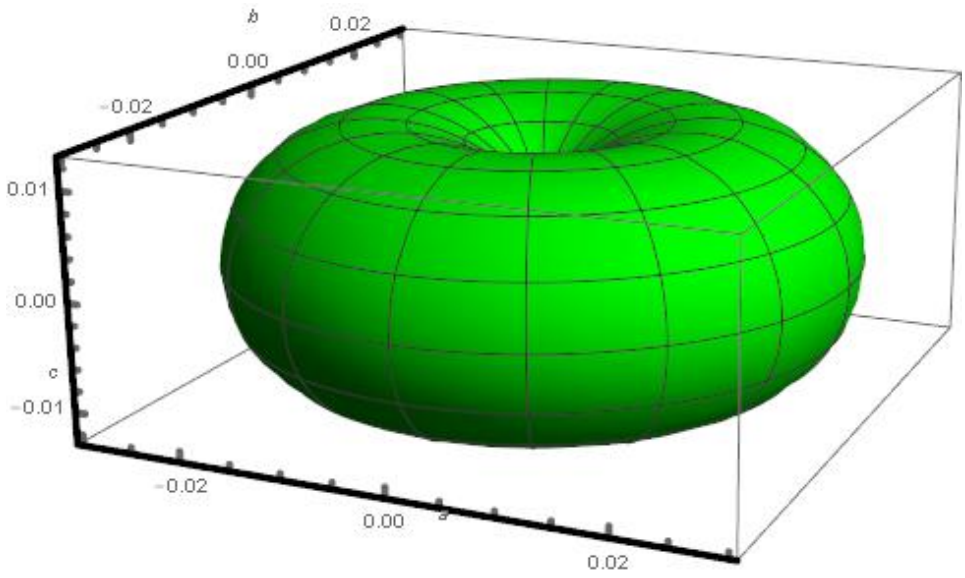

Figure. S5. 3-D linear compressibility representation surface $\beta(\theta, \varphi)$ of ZIF-zni in TPa^{-1}.

8 Poisson's Ratio 3-D Plot for ZIF-zni

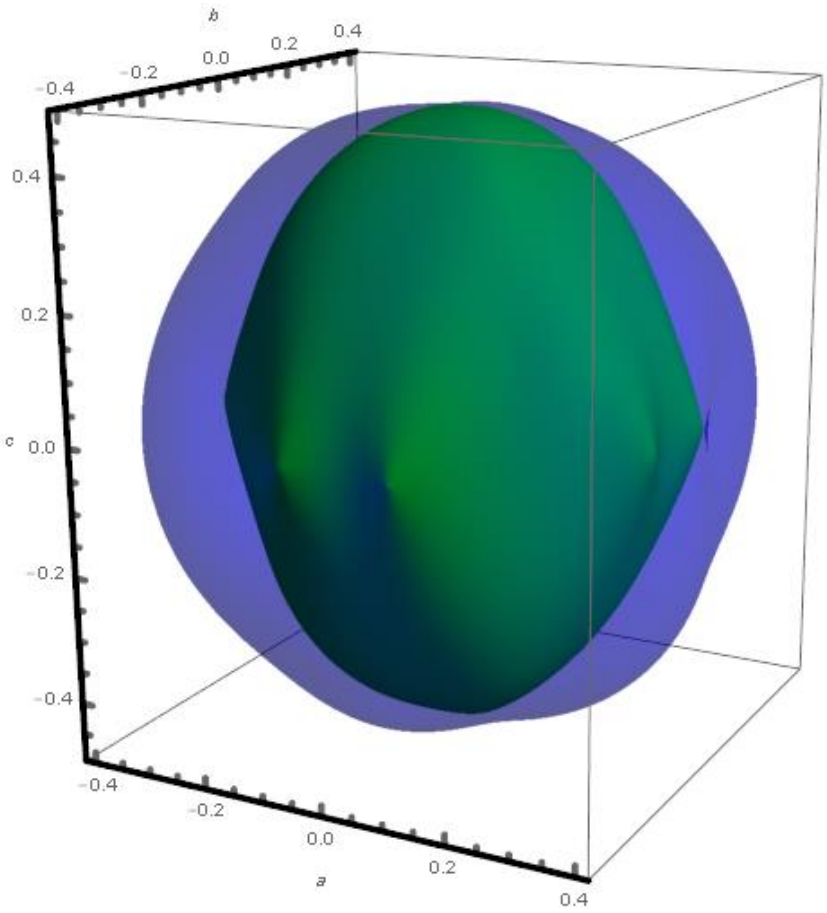

Figure. S6. 3-D Poisson's ratio representation surface $v(\theta, \varphi, \chi)$ of ZIF-zni. Colour coding used: blue and green represent the maximum and minimum values.

9 References

1. Bennett, T.D., et al., *Structure and properties of an amorphous metal-organic framework.* Phys Rev Lett, 2010. **104**(11): p. 115503.

2. Ryder, M.R., et al., *Identifying the role of terahertz vibrations in metal-organic frameworks: from gate-opening phenomenon to shear-driven structural destabilization.* Phys Rev Lett, 2014. **113**(21): p. 215502.

3. Park, K.S., et al., *Exceptional chemical and thermal stability of zeolitic imidazolate frameworks.* Proc Natl Acad Sci U S A, 2006. **103**(27): p. 10186-91.

4. Cinque, G., et al., *Multimode InfraRed Imaging and Microspectroscopy (MIRIAM) Beamline at Diamond.* Synchrotron Radiation News, 2011. **24**(5): p. 24-33.

5. Greenaway, A., et al., *In situ synchrotron IR microspectroscopy of CO2 adsorption on single crystals of the functionalized MOF Sc2(BDC-NH2)3.* Angew Chem Int Ed Engl, 2014. **53**(49): p. 13483-7.

6. Dovesi, R., et al., *CRYSTAL14: A program for the ab initio investigation of crystalline solids.* International Journal of Quantum Chemistry, 2014. **114**(19): p. 1287-1317.

7. Ryder, M.R. and J.C. Tan, *Explaining the mechanical mechanisms of zeolitic metal-organic frameworks: revealing auxeticity and anomalous elasticity.* Dalton Trans, 2016. **45**(10): p. 4154-61.

8. Perdew, J.P., K. Burke, and M. Ernzerhof, *Generalized Gradient Approximation Made Simple.* Physical Review Letters, 1996. **77**(18): p. 3865-3868.

9. Grimme, S., *Semiempirical GGA-type density functional constructed with a long-range dispersion correction.* Journal of Computational Chemistry, 2006. **27**(15): p. 1787-1799.

10. Becke, A.D., *Density-Functional Thermochemistry .3. The Role of Exact Exchange.* Journal of Chemical Physics, 1993. **98**(7): p. 5648-5652.

11. Ryder, M.R., B. Civalleri, and J.C. Tan, *Isoreticular zirconium-based metal-organic frameworks: discovering mechanical trends and elastic anomalies controlling chemical structure stability.* Phys Chem Chem Phys, 2016. **18**(13): p. 9079-87.

12. Ryder, M.R., et al., *Discovering connections between terahertz vibrations and elasticity underpinning the collective dynamics of the HKUST-1 metal-organic framework.* Crystengcomm, 2016. **18**(23): p. 4303-4312.